J|A|C|S
ARTICLES

Published on Web 05/07/2009

X-ray Crystal Analysis of a TASP: Structural Insights of a Cavitein Dimer

Jon O. Freeman,[‡] Woo Cheol Lee,[†] Michael E. P. Murphy,*[,†] and John C. Sherman*[,‡]

Department of Microbiology and Immunology, Life Sciences Institute, University of British Columbia, 2350 Health Sciences Mall, Vancouver, BC, Canada V6T 1Z3, and Department of Chemistry, University of British Columbia, 2036 Main Mall, Vancouver, BC, Canada V6T 1Z1

Received February 25, 2009; E-mail: Michael.Murphy@ubc.ca (M.E.M); Sherman@chem.ubc.ca (J.C.S)

Abstract: Cavitein Q4 is a template assembled synthetic protein designed for X-ray crystallographic analysis. It is based on a previous monomeric helical bundle cavitein (N1GG) that consists of four identical parallel helical peptides. Crystals that were grown in the presence of bromide ions were used to solve the initial phases via single-wavelength anomalous dispersion (SAD). A 1.4 Å resolution data set was then refined starting with the SAD phases to provide the crystal structure of cavitein Q4. The crystal structure revealed cavitein Q4 as an asymmetric dimer, although the cavitein appears to be largely monomeric in solution. A comparative analysis is carried out to discern any intrinsic differences between Q4 and its parent cavitein N1GG. We present herein the first X-ray crystal structure of a TASP system and relate this structure to the solution data for both Q4 and its parent N1GG.

Introduction

A comprehensive understanding of protein folding remains one of the great goals in science today. Since Anfinsen's folding experiment with ribonuclease, the scientific community has made great strides in understanding the complexity of how proteins fold.[1−6] In a recent paper, Service proposed that the major hurdles of protein folding have been largely solved by computational modeling.[7] Yet the challenges of designing or controlling a protein's folded state and function remain anything but trivial.

One approach toward investigating the protein folding problem is through the study of synthetic de novo (from scratch) proteins.[8−11] One of the pioneers of de novo protein design is DeGrado, who based his early work on a minimalist approach founded on first principles.[12,13] DeGrado illuminated the stage for synthetic proteins, and roughly 20 years later his work remains a keystone in de novo design strategies.

Shortly after DeGrado's initial work, Mutter introduced the template assembled synthetic protein (TASP) as a simple system for modeling and exploring the underlying principles that govern a protein's folded structure.[14,15] The advent of Mutter's first TASP augmented the emerging field of de novo protein science. Mutter et al. fashioned the first TASP from the covalent ligation of de novo peptides to a peptidic template to form a four-helix bundle mimetic.[15] Since Mutter's initial TASP, a multitude of groups have investigated super secondary and tertiary structural motifs through the use of simple de novo peptides attached to a diverse array of templates.[16−21] TASPs have since led to the understanding and creation of "native-like" synthetic protein systems.[22−24]

[†] Department of Microbiology and Immunology.
[‡] Department of Chemistry

(1) Sela, M.; White, F. H.; Anfinsen, C. B. *Science* **1957**, *125*, 691–692.
(2) Haber, E.; Sela, M.; White, F. H.; Anfinsen, C. B *Proc. Natl. Acad. Sci. U. S. A.* **1961**, *47*, 1309–1314.
(3) Venkatraman, J.; Shankaramma, S. C.; Balaram, P. *Chem. Rev.* **2001**, *101*, 3131–3152.
(4) Ghosh, K.; Ozkan, S. B.; Dill, K. A. *J. Am. Chem. Soc.* **2007**, *129*, 11920–11927.
(5) Dill, K. A.; Ozkan, S. B.; Shell, M. S.; Weikl, T. R. *Annu. Rev. Biophys.* **2008**, *37*, 289–316.
(6) Chen, Y.; Ding, F.; Nie, H.; Serohijos, A. W.; Sharma, S.; Wilcox, K. C.; Yin, S.; Dokholyan, N. V. *Arch. Biochem. Biophys.* **2008**, *469*, 4–19.
(7) Service, R. F. *Science* **2008**, *321*, 784–786.
(8) DeGrado, W. F. *Science* **1997**, *278*, 80–81.
(9) Hecht, M. H.; Das, A.; Go, A.; Bradley, L. H.; Wei, Y. *Protein Sci.* **2004**, *13*, 1711–1723.
(10) Monien, B. H.; Drepper, F.; Sommerhalter, M.; Lubitz, W.; Haehnel, W. *J. Mol. Biol.* **2007**, *371*, 739–753.
(11) Bender, G. M.; Lehmann, A.; Zou, H.; Cheng, H.; Fry, H. C.; Engel, D.; Therien, M. J.; Blasie, J. K.; Roder, H.; Saven, J. G.; DeGrado, W. F. *J. Am. Chem. Soc.* **2007**, *129*, 10732–10740.
(12) Degrado, W. F.; Wasserman, Z. R.; Lear, J. D. *Science* **1989**, *243*, 622–628.
(13) Regan, L.; Degrado, W. F. *Science* **1988**, *241*, 976–978.
(14) Mutter, M.; Altmann, E.; Altmann, K.; Hersperger, R.; Koziej, P.; Nebel, K.; Tuchsecherer, G.; Vuilleumier, S.; Gremlich, H.; Müller, K. *Helv. Chim. Acta* **1988**, *71*, 835–847.
(15) Mutter, M.; Vuilleumier, S. *Angew. Chem., Int. Ed.* **1989**, *28*, 535–554.
(16) Li, W.; Hellwig, P.; Ritter, M.; Haehnel, W. *Chem. -Eur. J.* **2006**, *12*, 7236–7245.
(17) Schneider, J. P.; Kelly, J. W. *Chem. Rev.* **1995**, *95*, 2169–2187.
(18) Akerfeldt, K. S.; Kim, R. M.; Camac, D.; Groves, J. T.; Lear, J. D.; DeGrado, W. F. *J. Am. Chem. Soc.* **1992**, *114*, 9656–9657.
(19) Ghadiri, M. R.; Soares, C.; Choi, C. *J. Am. Chem. Soc.* **1992**, *114*, 4000–4002.
(20) Lieberman, M.; Sasaki, T. *J. Am. Chem. Soc.* **1991**, *113*, 1470–1471.
(21) Wong, A. K.; Jacobsen, M. P.; Winzor, D. J.; Fairlie, D. P. *J. Am. Chem. Soc.* **1998**, *120*, 3836–3841.
(22) Tuchscherer, G.; Grell, D.; Mathieu, M.; Mutter, M. *J. Pept. Res.* **1999**, *54*, 185–194.
(23) Becker, C. F. W.; Oblatt-Montal, M.; Kochendoerfer, G. G.; Montal, M. *J. Biol. Chem.* **2004**, *279*, 17483–17489.

Scheme 1

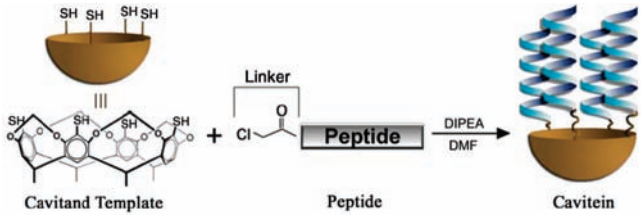

Distinguishing the folding of a synthetic de novo protein is imperative to fully appreciate the relationship between design and structure. For this reason, TASPs have been extensively characterized, with the exception of NMR solution determination or X-ray crystallography. However, solution and crystal structures have been successfully elucidated for de novo proteins by several groups.[25−29] Arleth et al. have recently proposed a low-resolution solution structure of a TASP via a combination of small-angle X-ray scattering (SAXS) and ab initio data analysis. These results provide exciting insight into the behavior of TASPs. The authors stress that subtle template variations have a marked affect upon the folded structure.

Calixarenes harboring mono- to tripeptides have been studied by Ungaro and Feigel in organic environments. Ungaro crystallized a calixarene with two dipeptides attached.[30] Feigel has characterized four dipeptides bound to a cavitand via NMR techniques and Monte Carlo calculations.[31] These examples are absent of secondary structural features and exposure to aqueous conditions. Currently the only progress in obtaining a TASP high resolution structure has been through the structure elucidation of peptide-free templates.[32,33] A well-defined high resolution TASP crystal or solution structure displaying both 2° and 3° structural elements remains to be solved.

A solution or crystal structure of a TASP would be a significant achievement toward the design of similar TASPs as it would elucidate structure to sequence relationships, shed light on other de novo/natural folding, depict the unnatural template to peptide liaison, and serve as a stepping stone for functionalizing the TASP for molecular recognition or enzymatic behavior.

Our group's TASPs often use a cavitand as the template, as they are rigid and can be readily linked to peptides (Scheme 1).[34−36] We have named these model systems "caviteins" from the combination of cavitand + protein.[37] Caviteins are typically helical bundles that owe their high thermostability to the template-driven saving of entropic cost of bundle organization. Other researchers have demonstrated the potential of peptides bound to cavitands and calixarenes as entities for protein surface recognition, highly selective small molecule binding, and antimicrobial activity.[38−41]

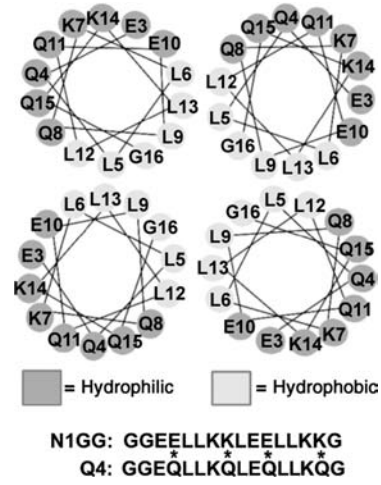

Figure 1. Helical wheel diagram depicting the amphiphilic design of the cavitein Q4 peptides.

Here we report a new cavitein, referred to as Q4, designed with the intent of growing crystals suitable for X-ray crystallography. The crystal structure of Q4 reveals a fascinating and unexpected dimeric TASP that is reminiscent of the recently reported eight helix β-peptide bundle reported by Schepartz et al.[42] The novel Q4 synthetic protein dimer may facilitate new venues and interest, but it also raises questions such as its bearing to our previous caviteins which we address here.

Results and Discussion

Design. The design of the Q4 and N1GG peptides, as described previously, was carried out in a minimalist fashion by limiting the variety of helical amino acids.[34] Leucine was incorporated for the hydrophobic component, and glutamate, lysine, and glutamine (in the case of Q4) were used for their hydrophilic character. The peptide was tailored to be amphiphilic by placing the hydrophobic leucines along one side of the α helix as depicted in Figure 1. Glutamate and lysine residues were placed on the opposing side in an i, i+4 relationship to favor intrahelical salt bridge stabilization.

N-terminal glycines were used as flexible linkers between the α helix and the cavitand template. The C-terminus was capped with a glycine residue to counter terminal helix fraying.[43]

(24) Hauert, J.; Fernandez-Carneado, J.; Michielin, O.; Mathieu, S.; Grell, D.; Schapira, M.; Spertini, O.; Mutter, M.; Tuchscherer, G.; Kovacsovics, T. *ChemBioChem* **2004**, *5*, 856–864.
(25) Sales, M.; Plecs, J. J.; Holton, J. M.; Alber, T. *Protein Sci.* **2007**, *16*, 2224–2232.
(26) Wei, Y.; Kim, S.; Fela, D.; Baum, J.; Hecht, M. H *Proc. Natl. Acad. Sci. U. S. A.* **2003**, *100*, 13270–13273.
(27) Karle, I. L.; Das, C.; Balaram, P *Proc. Natl. Acad. Sci. U. S. A.* **2000**, *97*, 3034–3037.
(28) Hill, R. B.; DeGrado, W. F. *J. Am. Chem. Soc.* **1998**, *120*, 1138–1145.
(29) Schafmeister, C. E.; LaPorte, S. L.; Miercke, L. J. W.; Stroud, R. M. *Nat. Struct. Mol. Biol.* **1997**, *4*, 1039–1046.
(30) Sansone, F.; Barboso, S.; Casnati, A.; Fabbi, M.; Pochini, A.; Ugozzoli, F.; Ungaro, R. *Eur. J. Org. Chem.* **1998**, *1998*, 897–905.
(31) Berghaus, C.; Feigel, M. *Eur. J. Org. Chem.* **2003**, *2003*, 3200–3208.
(32) Tsukamoto, K.; Ohishi, H.; Maezaki, N.; Tanaka, T.; Ishida, T. *ChemBioChem* **2006**, *7*, 1559–1562.
(33) Peluso, S.; Rückle, T.; Lehmann, C.; Mutter, M.; Peggion, C.; Crisma, M. *ChemBioChem* **2001**, *2*, 432–437.
(34) Mezo, A. R.; Sherman, J. C. *J. Am. Chem. Soc.* **1999**, *121*, 8983–8994.
(35) Huttunen-Hennelly, H. E. K.; Sherman, J. C. *Pept. Sci.* **2008**, *90*, 37–50.
(36) Seo, E. S.; Scott, W. R. P.; Straus, S. K.; Sherman, J. C. *Chem. -Eur. J.* **2007**, *13*, 3596–3605.
(37) Gibb, B. C.; Mezo, A. R.; Sherman, J. C. *Tetrahedron Lett.* **1995**, *36*, 7587–7590.
(38) Hamuro, Y.; Calama, M. C.; Park, H. S.; Hamilton, A. D. *Angew. Chem., Int. Ed.* **1997**, *36*, 2680–2683.
(39) Brewster, R. E.; Caran, K. L.; Sasine, J. S.; Shuker, S. B. *Curr. Org. Chem.* **2004**, *8*, 867–881.
(40) Hülsbusch, C. M.; Feigel, M. *J. Incl. Phenom. Macrocycl. Chem* **2007**, *59*, 53–63.
(41) Lazzarotto, M.; Sansone, F.; Baldini, L.; Casnati, A.; Cozzini, P.; Ungaro, R. *Eur. J. Org. Chem.* **2001**, *2001*, 595–602.
(42) Daniels, D. S.; Petersson, E. J.; Qiu, J. X.; Schepartz, A. *J. Am. Chem. Soc.* **2007**, *129*, 1532–1533.
(43) Aurora, R.; Srinivasan, R.; Rose, G. *Science* **1994**, *264*, 1126–1130.

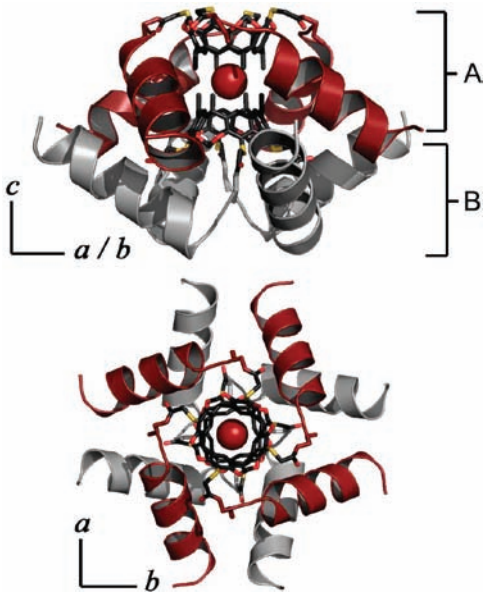

Figure 2. Cavitein Q4 dimer depicted from "side" (top) and "top" (bottom) views. Helical conformations A and B are colored red and silver, respectively. The red sphere between the cavitand feet is a bromide ion.

The C-terminus was also amidated to reduce the macrodipole effect and eliminate C-terminal charge−charge repulsion between neighboring helices. The tetrathiol cavitand was chosen for its rigidity and its four equivalently spaced nucleophilic sulfur functionalities.

Our goal was to obtain a crystal structure of our most native-like monomeric cavitein N1GG/Ar/Me (N1GG).[34] Crystallization of N1GG was precluded due most likely to its high solubility in water—32 charges spread over a molecular weight of ~8019. Glutamine residues were therefore chosen to replace two salt bridges per helix to reduce the solubility of N1GG while maintaining a hydrophilic character. This reduction of four charges per helix resulted in a net loss of 16 charges per cavitein thereby halving the overall charge of N1GG and giving rise to our new cavitein Q4.

Synthesis. Use of a Rink amide resin affords a peptide with a C-terminal amide. The N-terminus itself was chloroacetylated (Scheme 1) to activate the peptide for template ligation. Linkage of the activated peptides to the thiol functionalized bowls was performed under basic conditions to yield the four helix cavitein.

Crystal Structure. Cavitein Q4 crystallized in the tetragonal space group *I*4. Ordered bromide ions bound within the Q4 crystal lattice were used to calculate phases via single-wavelength anomalous dispersion (SAD) techniques. These phases were used to refine the structure of cavitein Q4 using a higher resolution data set to 1.40 Å. This high resolution structure will be discussed and presented herein. Due to pseudosymmetry, the *I*4 space group was chosen over *I*422, generating two different cavitein dimers; however, the difference between the two dimers in the refined structure is negligible (0.067 Å rms for Cα atoms).

Cavitein Dimer. Contained within a dimer are two unique helices (A and B), each covalently bound to one-quarter of the cavitand template, resulting in each Q4 cavitein monomer harboring either all A or all B helical conformations (Figure 2). Thus, each dimer is composed of an all A form cavitein and an all B form cavitein resulting in an asymmetric dimer. The principal axis with 4-fold rotational symmetry is the *c* axis which runs through the center of the cavitand template.

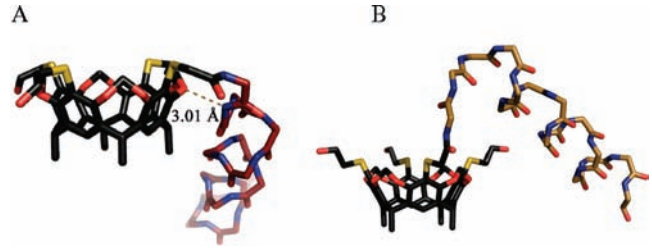

Figure 3. (a) Depiction of helix A immediately folding down toward the template feet. Also depicted is the potential hydrogen bonding between G2 and a template oxygen. (b) Depiction of helix B bound to the cavitand template. The linker region in helix B is seen extending up and away from the bowl before descending.

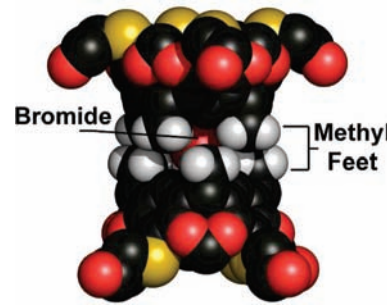

Figure 4. Depiction of the two cavitand templates positioned "feet to feet" in the dimeric cavitein structure. Hydrogens are depicted only for the methyl feet.

The Q4 cavitein X-ray crystal structure is unveiled as an asymmetric eight-helix bundle dimer. Monomers are distinguished by the differing connectivity of the helices to the template and the extent to which the cavitand bowls are buried in the core (Figures 2 and 3). Contrary to the expectation that the peptides would bundle above the template as depicted in Scheme 1, we see alternatively the peptides wrapping downward around the cavitand bowl. The helices of one cavitein monomer intercalate in an antiparallel helix arrangement with the helices of an opposing cavitein.

Peptide and Template Characteristics. Helices A and B differ in their connection to their cavitand template (Figure 3). Helix A is folded such that the spatial proximity between the amide nitrogen of G2 and a template oxygen appear to be hydrogen bonded.[34] This H-bond may contribute to the stability of the immediate downward fold seen by helix A. No peptide to template H-bonding is evident in helix B as the linker region extends away from the bowl.

The caviteins dimerize such that two cavitand templates interact feet to feet. The two cavitands are offset by 45° around the 4-fold rotational axis with respect to each other resulting in staggered methyl feet (Figure 4). Futhermore, the cavitands are encased by the helices and contribute to the interior hydrophobic core (Figure 2).

Interestingly, a bromide ion is bound between the eight methyl feet of the two cavitands. It is rare to see anion binding in such a hydrophobic environment. Schalley et al. have reported C−H···X anion interactions between the inward acetal hydrogens of a resorcinarene and an anion.[44] Calixarene anion binding is typically achieved via chelator functionalization or π-metalation.[45,46] However, to the best of our knowledge, an anion locked within a neutral cavitand's feet has not been documented. Interestingly, the electron density is present near the opposite face of the cavitand bowl, separated by 6.3 Å from the bromide

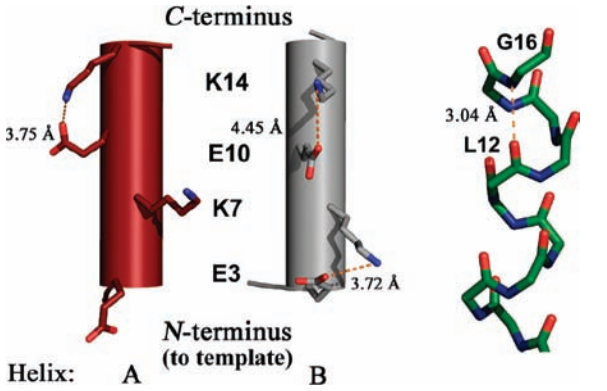

Figure 5. Left two helices depict distances between salt bridges E−K in helices A and B. From bottom to top: E3, K7, E10, K14. The helix on the right depicts G16 capping on helix B.

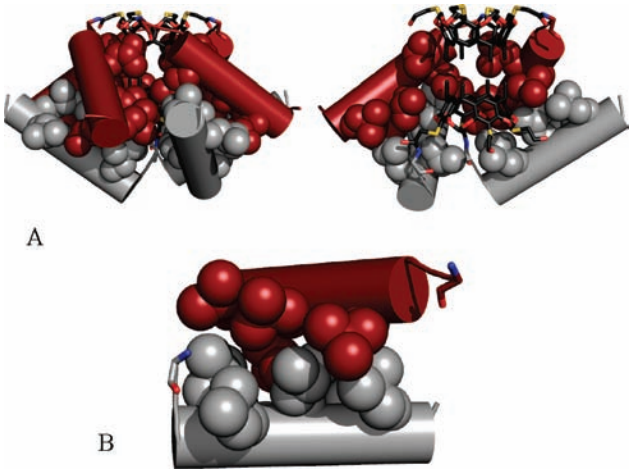

Figure 6. (A) Leucine side chain carbons are depicted as spheres along the cylindrically modeled alpha helices. The left image represents an exterior view of the cavitein. The right image is a cut away exposing the inside of the dimer. (B) Knobs-into-holes interhelical packing within the cavitein Q4 dimer.

ion. This density is identified as a sodium ion in our model, and we assume the ion is stabilized, in part, by the bromide ion. The presence of bromide in the crystallization conditions was found to provide larger crystals; however it is not required for crystal growth.

One of the minor differences between each of the helix side chains is in the intrahelical salt bridges. Helix A has one salt bridge between E10-K14, whereas E3 is rotated back toward the template (Figure 5). Both glutamate/lysine pairs on helix B suggest salt bridging as shown in Figure 6. Interpretations of the salt bridges should be taken lightly however, as a disordered density is manifest for each pair.

The glycine capping of the C-terminus to L12 is apparent in helix B and provides helix stabilization in TASP Q4 as designed (Figure 5).[43] The terminal glycine is unobservable in helix A presumably due to fraying.

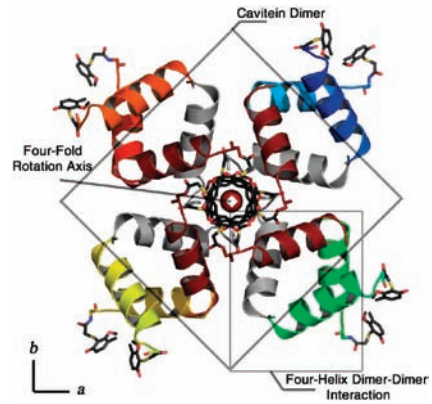

Figure 7. Views of the Cavitein Q4 dimer from the "top" interacting with neighboring Q4 dimers.

The Ramachandran plot (Figure S2 in Supporting Information) illustrates further structural validation for cavitein Q4 in both helix A and B conformations.[47,48] The residues of cavitein Q4 harbor phi/psi angles in preferred conformations and in accordance with alpha helices.

Intradimer Packing. Although the crystal structure is not a monomeric four-helix bundle as predicted, the original design of a bundled system with a hydrophobic core and hydrophilic exterior is maintained (Figure 6). Note how the leucines (depicted as spheres in Figure 6a) are located internally and are directed inward toward the cavitand template giving rise to a hydrophobic core.

The buried surface area of the residues was found to be 763 and 750 Å^2 for helix A and B, respectively (ca. ∼45%), from the program Areaimol.[49] This fits with our designed expectation where approximately half of the amphiphilic helix should be buried in a hydrophobic core.

Packing within the dimer is best described as a knobs-into-holes arrangement as seen in Figure 6. "Knobs" created by the leucine side chains on one helix are packed between the spacings, or "holes", found between neighboring side chains along an opposing helix.[50] The interhelical angle between dimer helices A and B was calculated to be 137° using the program HELIXANG from the CCP4 suite.[51]

Lattice Packing. A closer look at the crystal lattice reveals an integrated cavitein−cavitein interaction with neighboring dimers. Aside from the observed eight-helix dimer, a four-helix bundle (tetramer of caviteins) exists between neighboring dimers (Figure 7). This dimer−dimer interaction is 4-fold around each cavitein extending in the *a*/*b* plane of the lattice creating a sheet of dimers (discussed below). The cavitein dimer has 24% (453 Å^2) of its surface area attributed to lattice packing contacts.[49] These dimer−dimer interactions may also be stabilized by interhelical glutamine hydrogen bonding interactions (Figure S3 in Supporting Information).

The crystals generated from Q4 were relatively rigid when compared to typical protein crystals and exhibited significant resiliency toward being cut or broken apart, suggesting strong

(44) Zhu, S. S.; Staats, H.; Brandhorst, K.; Grunenberg, J.; Gruppi, F.; Dalcanale, E.; Lützen, A.; Rissanen, K.; Schalley, C. A. *Angew. Chem., Int. Ed.* **2008**, *47*, 788–792.
(45) Staffilani, M.; Hancock, K. S. B.; Steed, J. W.; Holman, K. T.; Atwood, J. L.; Juneja, R. K.; Burkhalter, R. S. *J. Am. Chem. Soc.* **1997**, *119*, 6324–6335.
(46) Lenthall, J. T.; Steed, J. W. *Coord. Chem. Rev.* **2007**, *251*, 1747–1760.
(47) Chothia, C.; Levitt, M.; Richardson, D *Proc. Natl. Acad. Sci. U. S. A.* **1977**, *74*, 4130–4134.
(48) Lovell, S. C.; Davis, I. W; Arendall, W. B.; Bakker, P. I. W. d.; Word, J. M.; Prisant, M. G.; Richardson, J. S.; Richardson, D. C. *roteins* **2003**, *50*, 437–450.
(49) Lee, B.; Richards, F. M. *J. Mol. Biol.* **1971**, *55*, 379–380.
(50) Efimov, A. V. *FEBS Lett.* **1999**, *463*, 3–6.
(51) , *Acta Crystallog. Sect. D* **1994**, *50*, 760–763, Collaborative Computational Project Number 4.

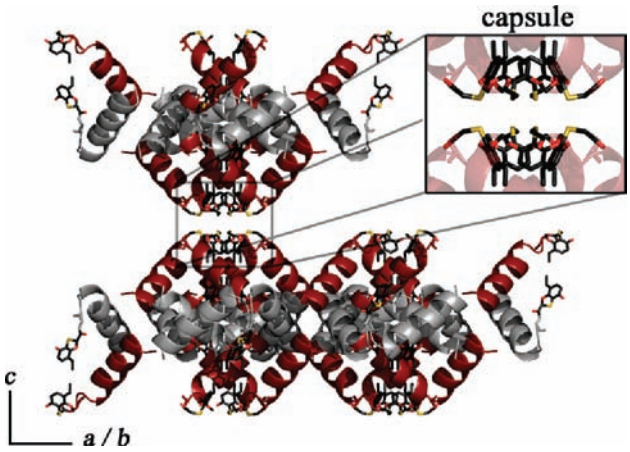

Figure 8. Expanded view of the Q4 crystal lattice depicting the "capsule" unit oriented between dimer sheets along the *a*/*b* plane (top).

crystal packing forces. This sparked intrigue into the lattice structure of our synthetic system and stimulated further exploration into its packing arrangement.

Noncovalent "capsules" formed by the alignment of the dimer−dimer sheets suggest the possibility of encapsulating small molecules within the crystal (Figure 8). Another interesting characteristic of the lattice is the large solvent channels typical of protein crystals (Figure S4 in Supporting Information). These channels are lined with the hydrophilic residues, run along both the *a* and *b* axis, and are oriented in a honeycomb pattern reminiscent of some zeolite structures.[52,53]

Looking down the *c* axis of the lattice reveals how the cavitand template creates pores through the sheets running along the *c* axis (Figure S4). These pores are rather small however, with respect to the pores along the *a*/*b* plane. The dimeric crystal structure and lattice prompted exploration into the behavior of cavitein Q4 in solution.

Analytical Ultracentrifugation. Sedimentation equilibrium experiments were carried out to address the issue of cavitein Q4's oligomeric state and relation to the parent sequence N1GG in solution. The Q4 sedimentation equilibrium data were found to fit a monomer−dimer model system with an association constant of 370 M^{-1} (Figure S5 in Supporting Information). This suggests Q4 exists primarily as a monomer at micromolar concentrations and 50% dimer at concentrations of ∼2.7 mM. Routine experiments such as circular dichroism (CD) and fluorescence are typically carried out at concentrations under 100 μM at which Q4 exists mainly as a monomer. NMR samples are routinely taken above 1 mM, at which cavitein Q4 will constitute an appreciable amount of dimer. Crystallization conditions were between 2.5 and 4.4 mM Q4 cavitein, where a dimeric structure was clearly accessible.

The oligomeric state of parent N1GG was reinvestigated for dimerization at high concentrations and was found to have a dimer association constant of 1250 M^{-1}. Therefore the removal of two salt bridges per helix with glutamine had a minimal effect on the aggregation potential of Q4 with respect to N1GG and, in fact, decreased it rather than increased it.

ANS Binding. The binding of 1-anilino-8-naphthalene sulfonate (ANS) is often used to probe the molten globule

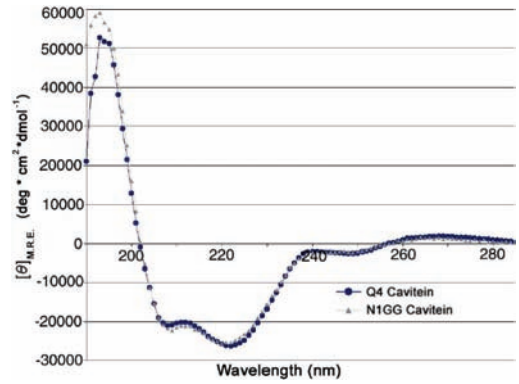

Figure 9. Far-UV CD spectra of cavitein Q4 and cavitein N1GG. Spectra were acquired at 25 °C in 50 mM phosphate buffer at pH 7.0 using a cavitein concentration of 40 μM.

characteristics of proteins by associating itself to exposed hydrophobic pockets.[54] Denatured proteins, however, will not bind ANS.

The only appreciable ANS binding observed for previous cavitein systems was by Seo et al. with five and six helical bundle cavitein systems.[55] ANS binding of these systems was attributed to a molten globule characteristic and the possibility of a hydrophobic cavity formed from the larger helical bundles.

In the case of Q4, ANS does not seem to bind appreciably at low concentrations of 35 μM (∼99% monomer) and 200 μM (∼88% monomer). However, upon increasing the concentration of Q4 to 1.25 mM (∼63% monomer), modest ANS binding is observed (Figure S6 in Supporting Information). There is a strong observable correlation between increasing dimer concentration with the increase of ANS fluorescence. Presumably, the weakly associating dimer provides a larger exposed hydrophobic environment for ANS to bind.[56,57]

N1GG was also investigated and showed similar behavior to Q4. N1GG's high concentration sample at 1.25 mM (∼43% monomer) bound more ANS than Q4 at the same concentration which should not be surprising, as N1GG is attributed with a higher association constant and thus a higher presence of dimer at similar concentrations. Our group has previously never tested caviteins for ANS binding under such concentrated conditions.

CD Spectra. Far-UV CD is used to characterize the secondary structural elements present in our caviteins. Cavitein Q4 displays characteristics of a typical helical peptide with minima at 222 and 208 nm and a maximum at 195 nm (Figure 9). Q4 has a nearly identical CD spectrum to N1GG and a helical content calculated to be ∼55%.[58,59] This similarity reasonably suggests that the alteration of salt bridges to glutamine pairs does not significantly affect the helicity of the peptide bundles.

The presence of near-UV CD bands is indicative of a defined tertiary structure.[60] Molten globule proteins often exhibit diminished or loss of signal in the near-UV region. Caviteins Q4 and N1GG display comparable near-UV CD bands which

(52) Madhusoodana, C. D.; Das, R. N.; Kameshima, Y.; Okada, K. *J. Porous Mater.* **2005**, *12*, 273–280.
(53) Onyestyák, G.; Valyon, J.; Papp, K. *Mater. Sci. Eng.: A* **2005**, *412*, 48–52.
(54) Matulis, D.; Baumann, C. G.; Bloomfield, V. A.; Lovrien, R. E. *Biopolymers* **1999**, *49*, 451–458.
(55) Seo, E. S.; Sherman, J. C. *Pept. Sci.* **2007**, *88*, 774–779.
(56) Johnson, M. L.; Formisano, S.; Edelhoch, H. *J. Biol. Chem.* **1978**, *253*, 1353–1356.
(57) Dusa, A.; Kaylor, J.; Edridge, S.; Bodner, N.; Hong, D.; Fink, A. L. *Biochemistry* **2006**, *45*, 2752–2760.
(58) Lee, D. G.; Park, Y.; Jin, I.; Hahm, K.; Lee, H.; Moon, Y.; Woo, E. *J. Pept. Sci.* **2004**, *10*, 298–303.
(59) Pace, C. N. *Methods Enzymol.* **1986**, *131*, 266–280.
(60) Kuwajima, K. *Proteins* **1989**, *6*, 87–103.

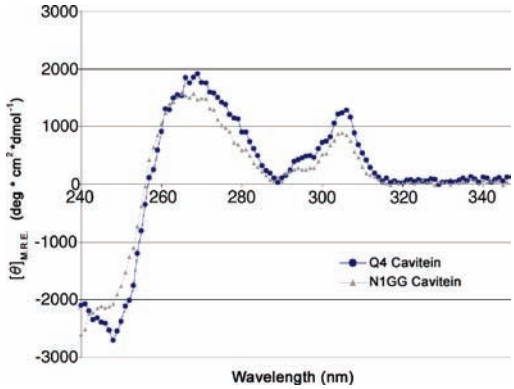

Figure 10. Near-UV CD spectra for cavitein Q4 and cavitein N1GG. Spectrum was acquired at 25 °C in 50 mM phosphate buffer at pH 7.0 using a cavitein concentration of 40 μM.

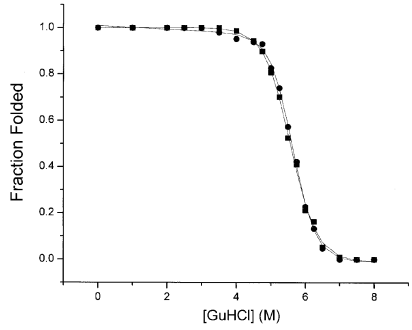

Figure 11. GuHCl denaturation curve of cavitein Q4 at both high (200 μM, ■) and low concentration (4 μM, ●). Each curve was acquired at pH 7.0 in 50 mM phosphate buffer at 25 °C.

Table 1. Calculated Values of $\Delta G°_{H_2O}$ for cavitein Q4 and N1GG

cavitein	$[GuHCl]_{1/2}$ (M)	m (kcal mol^{-1} M^{-1})	$\Delta G°_{H_2O}$ (kcal mol^{-1})
N1GG Mezo et al.	5.7 ± 0.1	−1.7 ± 0.1	−9.9 ± 0.3
N1GG Huttunen et al.	5.7 ± 0.1	−1.8 ± 0.1	−10.4 ± 0.3
Q4	5.6 ± 0.1	−1.7 ± 0.1	−9.6 ± 0.6

suggest similar tertiary folding behavior near the cavitand chromophore (Figure 10).

The thermodynamic stability of cavitein Q4 was examined via guanidine HCl denaturation and compared to cavitein N1GG. Denaturation was monitored by CD at $[\theta]_{222}$, and the data were assessed using nonlinear least-squares fitting (Figure 11). The calculated value of $\Delta G°_{H_2O}$ for cavitein Q4 is -9.6 ± 0.6 kcal mol^{-1}. This is within error of the previously reported values for N1GG by Mezo and Huttunen (Table 1).[34,35]

Concentration-dependent GuHCl unfolding experiments (high, 200 μM; low, 4 μM) were carried out to examine the aggregation state of Q4.[61] The high and low concentration studies showed indistinguishable denaturation curves, indicating that Q4 denatures cooperatively as a monomeric species (Figure 11). The low concentrations of cavitein used suggest only a modicum of dimer would be present. Therefore, initial GuHCl addition would likely disaggregate the trace dimer.

^{1}H NMR. Most native proteins display well dispersed proton signals, in contrast to molten globules which exhibit broad signals due to structurally averaged protein backbones. N1GG has ~14 dispersed amide signals (including the two NH_2 signals

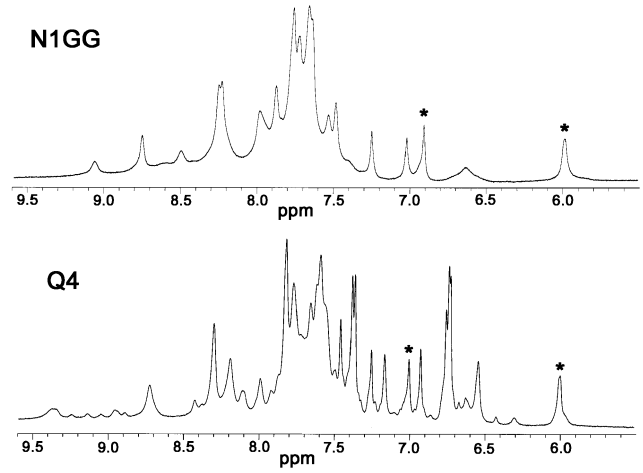

Figure 12. 1D 600 MHz ^{1}H NMR amide region for cavitein N1GG (top) and Q4 (bottom). Cavitand signals are marked via (*) in both cases. The spectra were recorded at 25 °C in phosphate buffer at pH 7.0 and 10% D_2O. The spectra shown above were taken at 225 μM (71% monomer) for N1GG and 350 μM (82% monomer) for Q4.

Table 2. Protection Factors for Caviteins Q4 an N1GG[a]

cavitein	first-order exchange rate (h^{-1})	half-life (h)	protection factor
N1GG	3.4×10^{-2}	20	$(6.3 \pm 0.4) \times 10^3$
Q4	9.2×10^{-2}	7.5	$(4.4 \pm 0.3) \times 10^3$

[a] Concentrations for N1GG and Q4 were 1.5 mM constituting 40% and 60% monomer, respectively.

from the C-terminus amide cap, but not including the two cavitand signals) (Figure 12). Q4 displays roughly 25+ amide signals. Due to the 4-fold symmetry of the cavitein, amide signals from glutamine side chains and glycine amide capping, ~26 amide signals should be seen for a symmetric species (Figure 12).

An examination of the kinetic stability of cavitein Q4 was carried out via N−H/D exchange experiments which investigated the protection factors of amide backbone protons to solvent exchange. Native alpha helical structures are tightly bound and held primarily by hydrogen bonding within the amide backbone. Thus, native-like structures will exchange amide protons more slowly than unfolded or molten globule proteins.[62] Native proteins have protection factors in the range 10^5-10^8, whereas those of molten globules are at 10^2-10^3.

Q4 cavitein was found to have a protection factor of $(4.4 \pm 0.3) \times 10^3$, which is comparable to N1GG, as shown in Table 2. These protection factors are typically considered in the high range of molten globule species, suggesting that the helices are unraveling/breathing to a certain extent. Protection factors in this range are commonly observed for well-defined de novo systems.

Comparison to Molecular Dynamic Simulations. In previous work, Seo et al. investigated cavitein structures by molecular dynamic simulations.[36,55,63] The molecular dynamics performed by Seo et al. were not set up to predict a dimer structure. However, significant tilting of the helical bundles in relation to the template was observed in the dynamic simulations. Hydrophobic shielding of the template via the helices may have

(61) Santoro, M. M.; Bolen, D. W. *Biochemistry* **1992**, *31*, 4901–4907.
(62) Englander, S. W.; Mayne, L.; Bai, Y.; Sosnick, T. R. *Protein Sci.* **1997**, *6*, 1101–1109.
(63) Scott, W. R. P.; Seo, E.; Huttunen, H.; Wallhorn, D.; Sherman, J. C.; Straus, S. K. *Proteins* **2006**, *64*, 719–729.

Table 3. X-ray Data Collection and Refinement Statistics for Cavitein Q4

	data refinement statistics	crystallographic data
	SSRL	SSRL
X-ray source	beamline 7_1	beamline 9_2
wavelength (Å)	0.9785	0.9188
temperature (K)	100	100
space group	*I*4	*I*4
cell dimensions (Å)		
a	45.33	45.51
b	45.33	45.51
c	74.95	74.20
resolution (Å)	38.8−1.40	38.87−1.60
highest resolution shell (Å)	1.45−1.40	1.68−1.60
total reflections	100 058	289 999
unique reflections	14 559	10 015
$I/\sigma(I)^a$	55.8 (5.6)	43.3 (19.3)
completeness(%)		
all data	97.4	99.6
last shell (Å)	87.7	99.7
multiplicity	6.9	29
$R_{merge}{}^a$ (%)	4.4 (34.9)	6.8 (20.5)
R (%)	18.7	
R_{free}(%)	19.9	
no. of protein atoms	488	
no. of cavitand template atoms	60	
no. of Br ions	2	
no. of Na ions	4	
no. of water molecules	32	
mean *B* values (Å^2)		
protein atoms	25.7	
cavitand template atoms	20.6	
Br ions	19.7	
Na ions	41.5	
water molecules	37.8	
rms deviation from ideal geometry		
bond lengths (Å)	0.014	
bond angles (deg)	1.36	

[a] Values listed in parentheses refer to the highest resolution bin.

occurred, as in the Q4 structure, if more time was carried out for the simulation. There is a renewed interest in how the dynamic simulations would result for various cavitein sequences if the current Q4 crystal structure is used as the starting frame.

Conclusion

Despite the apparent discrepancy in oligomeric states, the crystal data do not invalidate the solution data, nor do the solution data invalidate the crystal data. In many ways, they enhance each other and our understanding of Q4's behavior.

The sedimentation equilibrium experiments revealed that at high concentrations dimerization occurs for both N1GG and Q4. Given these results, it is not surprising to see a dimeric crystal lattice form from the highly concentrated crystal growth environment. The similarity in solution behavior between N1GG and Q4 via CD, ANS, sedimentation equilibrium, GuHCl, ^{1}H NMR, and N−H/D exchange experiments suggest that the replacement of salt bridges with glutamines had only a minor effect upon the cavitein structure. Thus, the design of cavitein Q4 afforded crystal growth due primarily to the decreased solubility from its parent N1GG sequence. The solution and crystal structure both validate the secondary α-helical structure, presence of salt bridges, glycine capping, and buried hydrophobic groups.

The resulting Q4 crystal structure offers new insights and will serve as a stepping stone into the design of future native-like caviteins. Knowledge of the spatial relationships between side-chain residues will imbue meaningful alterations to newly designed caviteins for the intent of dimer stabilization, lattice and crystal growth formation, monomer partiality, or cavitein functionalization. Attempts are currently underway to grow crystals of cavitein monomers, stabilized dimers, and previously assigned dimeric caviteins to compare their structural relation to the Q4 dimer.

Experimental Section

Peptide Synthesis. Standard solid-phase methods and the Fmoc/*t*-Bu strategy were used to synthesize all peptides on a C S Bio (Menlo Park, CA) 136XT peptide synthesizer. Rink's amide resin was used to afford C-terminal amides. All chemicals were purchased from Advanced Chemtech (Louisville, KY) and C S Bio, except for DMF and the activating reagents, which were purchased from Aldrich. The free N-terminus of the 16-amino acid peptide resin (500 mg resin, 374 mg peptide, 0.21 mmol) was reacted with chloroacetyl chloride (200 μL, 2.52 mmol) and DIEA (300 μL, 1.72 mmol) in dry DMF (5 mL) for 2 h at room temperature. Following activation with chloroacetyl chloride, each peptide resin was washed with dichloromethane (DCM), cleaved from the resin using a 1.5-h treatment of 95% TFA/H_2O solution, and purified by reversed-phase HPLC using a linear gradient of acetonitrile (0.05% TFA) and water (0.1% TFA) on a Waters C-18 Delta Pak column (300 × 19 mm^2, 300 Å, 15 μm) at a flow rate of 10 mL min^{-1}. Q4 peptide eluted at ∼64% H_2O starting with a gradient from 70% to 60% over 25 min. The purity of each peptide was assessed by the observation of a single peak by analytical reversed-phase HPLC (>95% pure). Purification by HPLC afforded the Q4 peptide as a white solid (∼160 mg). MALDI-TOF: *m*/*z* 1858 ($(M + H)^+$). The reported yields are only approximate due to adsorbed water present after lyophilization and variable loading of the peptide resin.

Cavitand Synthesis. The synthesis of the cavitand template has been previously described.[64]

Cavitein Synthesis. Purified peptide (6.5 equiv, 13.5 μmol) along with cavitand (1 equiv, 2.1 μmol) were dissolved in 1 mL of degassed DMF. DIPEA (115 μmol, 20 μL) was added to the solution and stirred overnight at room temperature. DMF was removed *en vacuo* to a final volume of ∼100 μL. The solution was diluted with H_2O and filtered with a 0.45 μm pore disposable filter. Cavitein Q4 was purified by reversed-phase HPLC on a Phenomenex Jupiter C-4 column (250 × 20 mm^2, 300 Å, 15 μm) with an acetonitrile (0.05% TFA) and water (0.1% TFA) solvent system. Cavitein Q4 eluted at ∼55% H_2O using a linear gradient from 65% to 48% H_2O. Cavitein Q4 purity was assessed by the observation of a single peak by analytical reversed-phase HPLC (>95% pure), and the identity was confirmed via mass spectrometry. MALDI-TOF: 8022 ($(M + K)^+$).

Cavitein Quantification. Cavitein Q4 was found to behave nonideally with conventional BCA and Bradford quantification assays. To circumvent this issue, a dichloromethane (DCM) standard of known concentration was injected into several NMR samples containing cavitein Q4 in deuterated methanol. The concentration of cavitein Q4 was then calculated based on the integration of DCM versus the cavitand signals in the ^{1}H NMR. The quantified cavitein Q4 stock solutions were subsequently used to determine an extinction coefficient of 9000 ± 400 M^{-1} cm^{-1} at 270 nm via a Perkin-Elmer UV/vis Lambda 2 spectrometer. This extinction coefficient was used as the primary means of cavitein Q4 quantification for the following experiments.

Circular Dichroism. The CD spectra were recorded on a JASCO J-710. Each spectrum was the result of averaging three scans, which were subtracted by the solvent baseline. All spectra were recorded at 25 °C with quartz cells of 1 mm or 1 cm path length. The

(64) Gibb, B. C.; Mezo, A. R.; Causton, A. S.; Fraser, J. R.; Tsai, F. C. S.; Sherman, J. C. *Tetrahedron* **1995**, *51*, 8719–8732.

instrument was calibrated routinely with *d*-10-(+)-camphorsulfonic acid. The recorded spectra were converted to mean residue ellipticity through the following equation:

$$[\theta] = \theta_{obs}/(10Cnl)$$

where θ_{obs} is the measured ellipticity in millidegrees, C is the concentration of the cavitein in M, n is the number of residues in the cavitein, and l is the path length in centimeters. Concentrations of cavitein Q4 varied from 200 μM to 4 μM in 50 mM phosphate buffer at pH 7.0.

GuHCl Denaturation. GuanidineHCl denaturation studies on cavitein Q4 were monitored via CD at $[\theta]_{222}$. The cavitein stock solution was prepared by dissolving purified cavitein in 50 mM phosphate buffer at pH 7.0. Subsequent dilution of the stock solution with 8 M GuHCl afforded data points ranging from 0 to 6 M GuHCl. Lyophilized stock cavitein solution followed by dilution of 8 M GuHCl and phosphate buffer concluded the following data points up to 8 M. $\Delta G°_{H_2O}$ was determined using the following equation

$$y = F(e^{-(G-mx)/RT}/(1 + e^{-(G-mx)/RT}))(1 - ax) + U(1 - (e^{-(G-mx)/RT}/(1 + e^{-(G-mx)/RT})))$$

where y is the fraction folded based on $[\theta]_{222}$ and x is equal to [GuHCl].[65] F, U, G, m, R, T, and a represent the least-squares analysis of pre- and post-translational $[\theta]_{222}$ intercepts, $\Delta G°_{H_2O}$, $\Delta G°$/[GuHCl], the universal gas constant, temperature, and a constant determined by least-squares analysis, respectively.

High and low cavitein concentrations (100, 40, and 4 μM) were carried out to examine any signs of aggregation. Three scans were taken with three different stocks of Q4 cavitein, and the errors were found to be within ± 5%.

NMR Spectroscopy. All NMR experiments were carried out at 298 K on a Bruker Avance 600 MHz spectrometer equipped with a 5 mm TCI (^{1}H ^{13}C/^{15}N) cryoprobe with an actively shielded /*Z*/-gradient. Water suppression was done using a presaturation pulse sequence with 32 scans, recycle delay of 2.5 s, and 32k time domain points. Presaturation was done using 59 dB attenuation on a 100 W amplifier. The proton 90° pulse was 9.5 μs (microseconds) at a pulse power of 3.5 dB.

Spectra were apodized by multiplication with an exponential decay corresponding to a 0.3 Hz line broadening in the transformed spectrum and a zero filling factor of 2. Spectra were processed using XWIN-NMR.

Samples were dissolved in 50 mM phosphate buffer (90:10, H_2O/D_2O) at pH 7.0. Concentrations of the caviteins were between 0.2 and 2.75 mM. The N−H/D exchange experiments were initiated by dissolving the cavitein directly into 50 mM acetic acid-d_4 buffer in D_2O at pD 5.0 and transferred quickly to an NMR tube. pD was corrected for isotope effects using the equation below.[66]

$$pD = pH(apparent) + 0.4$$

The first scan was acquired as soon as possible, followed by scans at arbitrary time increments. The signal heights were integrated and normalized with the nonexchangeable proton H_{out} (near 6 ppm) from the cavitand. Reference spectra were taken with cavitein Q4 in 50 mM acetate buffer (90:10 H_2O/D_2O) at 298 K. Protection factors were calculated using the equation

$$P = k_{int}/k_{ex}$$

where P is the protection factor, k_{int} is the intrinsic rate of exchange, and k_{ex} is the exchange rate of the observed amide proton.

Analytical Ultracentrifugation. A Beckman Coulter Optima XL-I analytical ultracentrifuge was used to carry out sedimentation equilibrium experiments. The rotor used was either an An60 Ti 4-hole or an An50 Ti 8-hole sample holder. Cavitein Q4 was dissolved in 50 mM phosphate buffer (pH = 7.0) in concentrations of 20, 40, 60 μM and 60, 80, 100 μM.

A 12 mm Epon centerpiece with six-sector cells was loaded with 3 × 120 μL samples at different concentrations and 3 × 130 μL of reference buffer. Data were equilibrated at three different rotor speeds of 25 000, 35 000, and 45 000 rpm at 20 °C. Samples equilibrated for 40 h and single scans 3 h apart were overlaid to conclude whether equilibrium had been reached. Scans were performed by measuring the absorbance at 270 nm with a step size of 0.001 cm, with 10 replicate scans. The partial specific volume for Q4 cavitein was determined based on the amino acid composition using the program SEDNTERP.[67] The data were fit to a monomer−dimer equilibrium using SEDPHAT.[68]

ANS Binding. Fluorescence experiments were carried out on a Varian CARY Eclipse fluorescence spectrophotometer equipped with a Xenon Arc lamp. Cavitein samples were taken up in a 50 mM phosphate buffer at pH 7.0 with concentrations ranging from 35 μM to 1.25 mM. All experiments were conducted at 20 °C using a 1 cm path length. The excitation wavelength was set at 370 nm, and the recorded emission range was taken from 385 to 600 nm. Reference spectra consisted of a 95% ethanol/5% water solution and 100% HPLC-grade methanol. All samples were prepared with a final concentration of 2 μM ANS.

Crystallization. Crystals were grown by the vapor diffusion hanging drop technique at room temperature. The drops consisted of 1 μL of cavitein solution (25 mg/mL in 10 mM MOPS) and 1 μL of reservoir solution containing 2.25 M ammonium sulfate, 0.1 M sodium acetate buffer at pH 5.2, and 0.1 M NaBr. Colorless crystals grew in ~1 day. Cavitein crystals grown for bromide SAD phasing consisted of 1 μL of cavitein solution (35 mg/mL in 10 mM MOPS) and 1 μL of reservoir solution containing 2.0 M ammonium sulfate, 0.1 M sodium acetate buffer at pH 4.7, and 1.0 M NaBr.

Data Collection and Analysis. X-ray diffraction experiments were carried out at the Stanford Synchrotron Radiation Laboratory (Palo Alto, CA). Crystals were soaked in a 24% (v/v) glycerol cryoprotectant prepared from the crystallization mother liquor and immersed in liquid nitrogen. The data were collected at 100 K.

An SAD experiment was conducted for bromide phasing using a data set collected at a wavelength of 0.9188 Å. For this data set, the crystal was grown in the presence of 1.0 M NaBr. A native data set was collected using radiation with a wavelength of 0.9785 Å and a crystal grown in the presence of 0.1 M NaBr. HKL2000 was used to index, scale, and integrate the data sets.

Structure Determination and Refinement. SAD phasing was used to solve the initial phases for cavitein Q4. The heavy atom search and the phasing were carried out with SHELXC/D/E as part of the CCP4 software.[51,69] Briefly, SHELXC/D was run to analyze the data set and locate the Br ion sites. The structure was determined in space group *I*422, and the phasing and density modification by SHELXE yielded easily identifiable structural features in the electron density map, including the helices of Q4 (Figure S7 in the Supporting Information). ARP/WARP was used to build an initial model.[70] A cif library was generated for the cavitand template refinement using PRODRG.[71,72] Model building was done using XtalView and COOT.[73,74] Restrained refinement and anisotropic

(65) Regan, L.; Rockwell, A.; Wasserman, Z.; DeGrado, W. *Protein Sci.* **1994**, *3*, 2419–2427.
(66) Glasoe, P. K.; Long, F. A. *J. Phys. Chem.* **1960**, *64*, 188–190.
(67) Lebowitz, J.; Lewis, M. S.; Schuck, P. *Protein Sci.* **2002**, *11*, 2067–2079.
(68) Schuck, P. *Anal. Biochem.* **2003**, *320*, 104–124.
(69) Sheldrick, G. M. *Acta Crystallogr. Sect. D* **2008**, *64*, 112–122.
(70) Perrakis, A.; Morris, R.; Lamzin, V. S. *Nat. Struct. Biol.* **1999**, *6*, 458–463.
(71) Schuettelkopf, A. W.; van Aalten, D. M. F. *Acta Crystallogr. Sect. D* **2004**, *60*, 1355–1363.
(72) Kleywegt, G. J.; Henrick, K.; Dodson, E. J.; van Aalten, D. M. F. *Structure* **2003**, *11*, 1051–1059.
(73) McRee, D. E. *J. Mol. Graphics* **1992**, *10*, 44–46.
(74) Emsley, P.; Cowtan, K. *Acta Crystallogr. Sect. D* **2004**, *60*, 2126–2132.

B-factor refinement were performed by REFMAC5.[75] The space group was changed to a lower symmetry of *I*4 during the refinement to yield a significantly better R_{free} (5% of the reflections were set aside for the cross validation). Bromide ion positions were confirmed by inspection of phased anomalous dispersion density maps. The resulting structural model is complete except for the terminal glycine of helix B. Crystallographic data and refinement statistics are shown in Table 3.

Acknowledgment. We would like to thank the Natural Sciences and Engineering Research Council of Canada (N.S.E.R.C.) for financial support, the Centre for Biothermodynamics and support from the Michael Smith Foundation for Health Research for the data collected on the analytical ultracentrifuge, F. Rossel and G. Mauk for use of the Varian Eclipse fluorimeter and Varian Cary4000 UV/vis absorption spectrophotometer, Z. Danilovic, and M. Ezhova for acquiring ^{1}H NMR spectra, and M. Scofield, L. Creighton, B. Lelj-Garolla, B. Patrick, and S. Strauss for their valuable discussions. This work was partially conducted at the Stanford Synchrotron Radiation Laboratory, a national user facility operated by Stanford University on behalf of the U.S. Department of Energy, Office of Basic Energy Sciences. The SSRL Structural Molecular Biology Program is supported by the Department of Energy, Office of Biological and Environmental Research, and by the National Institutes of Health, National Center for Research Resources, Biomedical Technology Program, and the National Institute of General Medical Sciences.

(75) Murshudov, G. N.; Vagin, A. A.; Dodson, E. J. *Acta Crystallogr. Sect. D* **1997**, *53*, 240–255.

Supporting Information Available: CCDC 726793 contains the supplementary crystallographic data for this paper. These data can be obtained free of charge via www.ccdc.cam.ac.uk/data_request/cif, or by emailing data_request@ccdc.cam.ac.uk, or by contacting The Cambridge Crystallographic Data Centre, 12, Union Road, Cambridge CB2 1EZ, UK; fax: +44 1223 336033. Unit cell, Ramachandran plot, dimer−dimer interactions, crystal lattice, sedimentation equilibrium data, ANS binding spectra, and electron density map identifying structural features. This material is free of charge via the Internet at http://pubs.acs.org.

JA901404W